MMSE SUBCARRIER EQUALIZATION FOR FILTER BANK BASED MULTICARRIER SYSTEMS

Dirk S. Waldhauser, Leonardo G. Baltar and Josef A. Nossek

Technische Universität München
Institute for Circuit Theory and Signal Processing
Arcisstr. 21, 80290 München, Germany
Email: {waldhauser, leo.baltar, josef.a.nossek}@tum.de

ABSTRACT

Filter bank based multicarrier systems (FBMC) offer a number of benefits over conventional orthogonal frequency division multiplexing (OFDM) with cyclic prefix (CP). One benefit is the improved spectral efficiency by not using a redundant CP and by having much better control of out-of-band emission. Another advantage is the ease of accomodating multiple users in an FDMA fashion especially in the uplink, i. e. the multiple access channel (MAC). On the other hand, more elaborate equalization concepts are needed compared to the single-tap per-subcarrier equalizer sufficient in the OFDM with CP case.

In this contribution we will present an efficient linear minimum mean square error (MMSE) equalization concept. Since FBMC systems employ Offset-Quadrature-Amplitude-Modulation (OQAM), a fractionally spaced per-subcarrier equalizer will be derived, which takes into account the inter-subcarrier interference due to frequency selective multipath fading. Still this is handled with decoupled per-subcarrier equalizers. Simulation results will show that OQAM-FBMCs allow for savings in transmit power which have to be paid with a practicable amount of computational overhead.

Index Terms— Signal processing, broadband communication systems, subcarrier multiplexing, equalizers, Wiener filtering

1. INTRODUCTION

Multicarrier systems provide many attractive properties for high rate wireless and wireline communication systems [1, 2]. Therefore, many current standards like HIPERLAN/2, IEEE 802.11 (WiFi), IEEE 802.16 (WiMAX), DVB and xDSL use multicarrier modulation. Moreover, multicarrier systems are very prominent candidates for the next generation of mobile communication systems (3GPP long-term evolution (LTE)). The mentioned standards are based on OFDM with CP. OFDM is on the one hand very popular because of the simple equalization enabled by the use of a CP as long as it covers the impulse response of the channel. On the other hand it decreases the scarce and expensive resource "bandwidth". The poor stopband attenuation of the subcarrier filters deteriorates the spectral efficiency by producing considerable levels of out-of-band radiation [3].

Complex modulated FBMC systems benefit from the design of frequency localized subcarrier filters which only overlap with their adjacent subcarriers. The overlap ensures an efficient use of the bandwidth whereas the stopband attenuation alleviates the problem of narrowband interferers, out-of-band radiation and the equalization of interchannel interference. We refrain from using perfect reconstruction subcarrier filters because the channel destroys this property anyway. For simplicity and due to satisfying results we use truncated square root raised cosine (RRC) FIR filters instead.

It is known from the theory of filter banks and transmultiplexers that prototype filters of exponentially modulated filter banks whose length exceeds the number of subcarriers M have to be implemented in an orthogonally staggered way which leads to orthogonally multiplexed QAM filter banks [2]. Our derivations of the equalizer solutions will be restricted to OQAM filter banks.

The authors of [4] have given a very efficient implementation by the use of the polyphase decomposition known as Modified DFT filter banks (MDFT).

In [1] and the references therein some solutions for the channel equalization in FBMC systems are given. Most of them are not satisfactory in the sense that they either aim at equalizing the frequency response of each subcarrier, work at the symbol rate or use adjacent subcarriers [5]. Equalizing the frequency response does not allow for a direct control of the residual interference in the output signal. Working at the symbol rate suffers from irrevocable aliasing or ICI in the signal whereas utilizing adjacent subcarriers elevates the complexity.

1.1. Notation

In the following sections we will use the convenient notation: The real and imaginary part of a signal, an impulse response or any matrix are written as $\mathrm{Re}[(\bullet)] = (\bullet)^{(\mathrm{R})}$ and $\mathrm{Im}[(\bullet)] = (\bullet)^{(\mathrm{I})}$, which means that $(\bullet) = (\bullet)^{(\mathrm{R})} + \mathrm{j}\,(\bullet)^{(\mathrm{I})}$, with $\mathrm{j} = \sqrt{-1}$. Vectors with a time index like $\boldsymbol{x}[n]$ are always compact notations for the $(N+1)$-dimensional vector $\big[x[n], x[n-1], \ldots, x[n-N]\big]^{\mathrm{T}}$, where N is explicitly given each time. $\boldsymbol{I}_N$ denotes the $N \times N$ identity matrix and $\boldsymbol{e}_\nu$ the unit vector with unity at the ν-th position.

2. STRUCTURE OF THE FBMC SYSTEM

The structure of the FBMC system is depicted in Fig. 1. The synthesis filter bank (SFB) combines the M low rate subcarrier signals into one high rate signal which is transmitted over a frequency selective radio channel. Additive white Gaussian noise (AWGN) is added at the receiver input. The receiver consists of an analysis filter bank (AFB) which splits the received high rate signal into M low rate subcarrier signals again. One FIR equalizer per subcarrier is employed to compensate for the intersymbol (ISI) and interchannel interference (ICI) caused by the frequency selective radio channel and improve the symbol decisions.

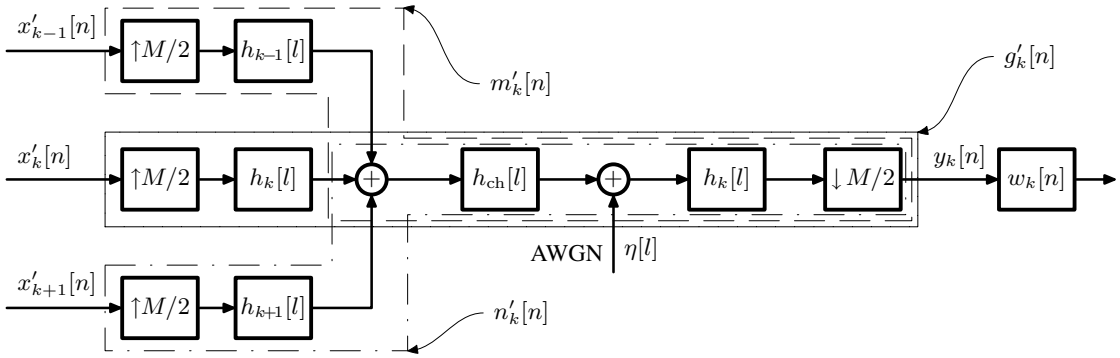

Fig. 2. Subcarrier Model for the FBMC System

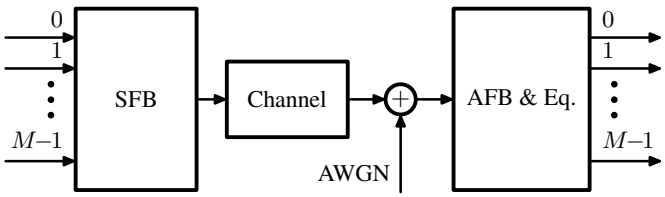

Fig. 1. FBMC System Overview

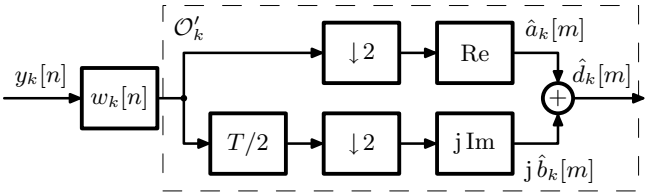

Fig. 3. OQAM Destaggering $\mathcal{O}'_k, k$ even

SFB and AFB are very efficiently implemented as Modified DFT (MDFT) filter banks [4] which make use of the exponential modulation

$$h_k[l] = h_0[l] \exp\left(\mathrm{j}\, 2\pi k l/M\right), \quad l = -KM/2, \ldots, KM/2 \quad (1)$$

and the polyphase decomposition of the zero-phase prototype filter $h_0[l]$ with length $KM + 1$. Details of the SFB and AFB block with equalization are given in the next section, but without using the efficient implementation.

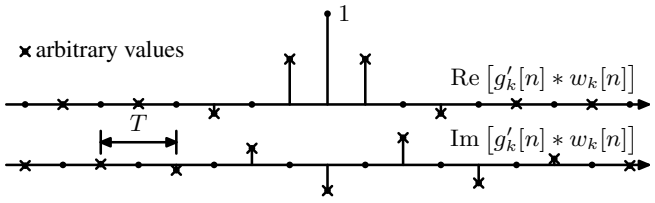

Fig. 4. Desired OQAM Impulse Response

3. EQUALIZER CALCULATION

The equalizer is necessary in order to remove the ISI and ICI caused by the frequency selective Rayleigh fading channel without inserting any redundancy in the sense of a guard interval like the CP. In this section we derive the equations for the linear MMSE equalizer and give the motivation for the used parameters and properties of the equalizer. The main aspects for the equalizer design are depicted in Fig. 2. We use only one equalizer per subcarrier, i. e. only the output signal of the corresponding subcarrier at the receiver is used for the estimation of the transmit symbols in order to achieve a low complexity. The complexity is, therefore, linear in terms of the subcarriers M and linear in terms of the equalizer coefficients N.

Nevertheless, the $T/2$ spacing of the equalizer allows for practically removing the ICI of the adjacent subcarrier signals at the receiver. This means that the orthogonality of OQAM systems can be recovered again. The ICI of non-adjacent subcarriers is controlled by the high stopband attenuation of the subcarrier filters with roll-off $\rho \leq 1$. Because of the orthogonal multiplexing of the subcarrier signals we have to modify the conventional MMSE equalization. Fig. 3 illustrates that the $\mathrm{Re}[\bullet]$ operation does not account for any information in the imaginary part and thus the equalizer should not force the imaginary part to zero in this case. It should produce an overall equalized impulse response $g'_k[n] * w_k[n]$ (Fig. 2) of the M OQAM multiplexed subcarriers as given in the example in Fig. 4. The stems with x-mark are allowed to possess arbitrary values, whereas those with filled circles have to be zero (except the one which is unity). This is necessary to avoid ISI after the downsampling by 2 and the real and imaginary part operations (cf. Fig. 3). The difference to conventional QAM systems is that the imaginary part of the impulse response is shifted relative to the real part by one time period. It is easily seen that this equalization concept can also be used in OQAM single carrier systems in a very similar way to [6]. The crucial idea in the application of multicarrier systems is that the ICI of adjacent subcarriers can also be introduced in the optimization procedure.

We, therefore, use the statistical information on the immediately adjacent subcarrier symbols in order to get a regularization term for the resulting Wiener-Hopf equation of the MSE minimization. Thus the interference is taken into account in the optimization process very similar to the noise. Again, the high stopband attenuation allows for omitting information about further subcarriers for the sake of low complexity.

In the following we will split complex symbols and filter coeffi-

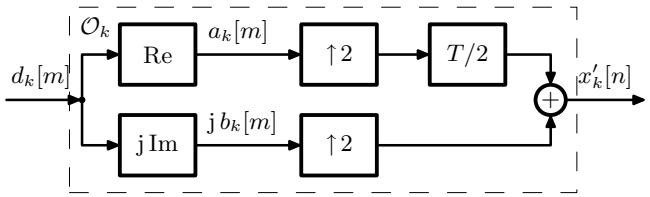

Fig. 5. OQAM Staggering $\mathcal{O}_k$, k even

cients into real and imaginary parts to account for the OQAM operations. The spectral shaping of the subcarrier filters leads to a strong simplification of the equalizer. Since there is only significant overlap between immediately adjacent subcarriers we can approximate the vector of the received subcarrier signal $\boldsymbol{y}_k[n] \in \mathbb{C}^N$ by

$$\boldsymbol{y}_k[n] \approx \boldsymbol{G}'_k \boldsymbol{x}'_k[n] + \boldsymbol{M}'_k \boldsymbol{x}'_{k-1}[n] + \boldsymbol{N}'_k \boldsymbol{x}'_{k+1}[n] + \boldsymbol{\Gamma}_k \boldsymbol{\eta}[l]. \quad (2)$$

$\boldsymbol{x}'_k[n] \in \mathbb{C}^{L+1}$ is given by the following equation and also illustrated in Fig. 5

$$\boldsymbol{x}'_k[n] = \begin{cases} \left[a_k[m],\, \mathrm{j}\, b_k[m],\, a_k[m-1],\, \ldots, x'_k[n-L]\right]^{\mathrm{T}}, & k \text{ even}, \\ \left[\mathrm{j}\, b_k[m],\, a_k[m],\, \mathrm{j}\, b_k[m-1],\, \ldots, x'_k[n-L]\right]^{\mathrm{T}}, & k \text{ odd}. \end{cases} \quad (3)$$

The last element of $\boldsymbol{x}'_k[n]$ depends on L and k according to Table 1.

$x'_k[n-L]$	L even	L odd
k even	$a_k[m - \lfloor (L/2) \rfloor]$	$\mathrm{j}\, b_k[m - \lfloor (L/2) \rfloor]$
k odd	$\mathrm{j}\, b_k[m - \lfloor (L/2) \rfloor]$	$a_k[m - \lfloor (L/2) \rfloor]$

Table 1. Last Element of Vector $\boldsymbol{x}'_k[n]$

Note that according to the characteristics of the OQAM-FBMC the role of the real and imaginary part operators are interchanged from subcarrier to subcarrier. This certainly holds true for the destaggering $\mathcal{O}'_k$ in Fig. 3. $\boldsymbol{G}'_k$, $\boldsymbol{M}'_k$ and $\boldsymbol{N}'_k \in \mathbb{C}^{N \times (L+1)}$ are the corresponding convolution matrices belonging to the impulse responses $g'_k[n], m'_k[n]$ and $n'_k[n]$ with length Q (cf. Fig. 2), which determines $L = N + Q - 2$. $\boldsymbol{\Gamma}_k$ comprises the filtering of the noise with $h_k[l]$ and the downsampling by $M/2$ and colorizes the white Gaussian noise $\eta[l]$.

The output of the AFB subcarrier filters $y_k[n]$ is then filtered by the subcarrier equalizer $w_k[n]$ of length N. The resulting subcarrier signal is destaggered by $\mathcal{O}'_k$, which downsamples the signal by two and gives the estimation $\hat{a}_k[m]$ by the real part and $\hat{b}_k[m]$ by j times the imaginary part as depicted in Fig. 3.

We can write the filter operation in vector notation as

$$\begin{aligned} \mathrm{Re}\left[\boldsymbol{w}_k^{\mathrm{H}} \boldsymbol{y}_k[n]\right] &= \boldsymbol{w}_k^{(\mathrm{R}),\mathrm{T}} \boldsymbol{y}_k^{(\mathrm{R})}[n] + \boldsymbol{w}_k^{(\mathrm{I}),\mathrm{T}} \boldsymbol{y}_k^{(\mathrm{I})}[n] \\ &= \hat{a}_k[m], \quad n = 2m, \quad m \in \mathbb{Z}, \end{aligned} \quad (4)$$

$$\begin{aligned} \mathrm{Im}\left[\boldsymbol{w}_k^{\mathrm{H}} \boldsymbol{y}_k[n-1]\right] &= \boldsymbol{w}_k^{(\mathrm{R}),\mathrm{T}} \boldsymbol{y}_k^{(\mathrm{I})}[n-1] - \boldsymbol{w}_k^{(\mathrm{I}),\mathrm{T}} \boldsymbol{y}_k^{(\mathrm{R})}[n-1] \\ &= \hat{b}_k[m], \quad n = 2m, \quad m \in \mathbb{Z}. \end{aligned} \quad (5)$$

Our design criterion is to minimize the mean square error between the estimated signal $\hat{d}_k[m] = \hat{a}_k[m] + \mathrm{j}\, \hat{b}_k[m]$ and the input signal $d_k[m] = a_k[m] + \mathrm{j}\, b_k[m]$. This solution is also obtained by

$$\boldsymbol{w}_{k,\mathrm{MMSE}} = \arg\min_{\boldsymbol{w}_k} \mathrm{E}\left[|\hat{a}_k[m] - a_k[m-\nu]|^2\right], \quad (6)$$

if $a_k[m]$ and $b_k[m]$ are wide sense stationary (WSS) and uncorrelated, i. e. $\mathrm{E}\left[a_k[m] b_k[m+m']\right] = 0, \forall m' \in \mathbb{Z}$. $\hat{a}_k[m]$ is a function of the equalizer coefficients $w_{k,n}$. The delay ν depends on the filters, the equalizer and the propagation channel and can be optimized for miminizing the MSE. We have used a fixed value throughout the simulations in Section 4. Using $\hat{b}_k[m]$ and $b_k[m-\nu]$ instead of $\hat{a}_k[m]$ and $a_k[m-\nu]$ in (6) leads to the same result for $\boldsymbol{w}_{k,\mathrm{MMSE}}$. This can also be understood by investigating Fig. 4 again and realizing that a filter $w_k[n]$ which produces this impulse response avoids ISI both for $a_k[m]$ and $b_k[m]$ in combination with $\mathcal{O}_k$ and $\mathcal{O}'_k$.

$\boldsymbol{y}_k^{(\mathrm{R})}[n]$ and $\boldsymbol{y}_k^{(\mathrm{I})}[n]$ in (4) and (5) can be further substituted by

$$\begin{aligned} \boldsymbol{y}_k^{(\mathrm{R})}[n] = \mathrm{Re}\left[\boldsymbol{y}_k[n]\right] \approx \boldsymbol{G}_k^{(\mathrm{R})} \boldsymbol{x}_k[n] + \\ \boldsymbol{M}_k^{(\mathrm{R})} \boldsymbol{x}_{k-1}[n] + \boldsymbol{N}_k^{(\mathrm{R})} \boldsymbol{x}_{k+1}[n] + \mathrm{Re}\left[\boldsymbol{\Gamma}_k \boldsymbol{\eta}[l]\right] \end{aligned} \quad (7)$$

and

$$\begin{aligned} \boldsymbol{y}_k^{(\mathrm{I})}[n] = \mathrm{Im}\left[\boldsymbol{y}_k[n]\right] \approx \boldsymbol{G}_k^{(\mathrm{I})} \boldsymbol{x}_k[n] + \\ \boldsymbol{M}_k^{(\mathrm{I})} \boldsymbol{x}_{k-1}[n] + \boldsymbol{N}_k^{(\mathrm{I})} \boldsymbol{x}_{k+1}[n] + \mathrm{Im}\left[\boldsymbol{\Gamma}_k \boldsymbol{\eta}[l]\right], \end{aligned} \quad (8)$$

which are obtained by taking the real and imaginary part of (2).

Note that $\boldsymbol{x}_k[n]$ is now calculated from (2) and (3) by shifting the j of each imaginary entry of $\boldsymbol{x}'_k[n]$ into the matrix $\boldsymbol{G}'_k$, which gives matrix $\boldsymbol{G}_k$. The same is true for $\boldsymbol{M}_k$ and $\boldsymbol{N}_k$. The dimensions do not change, but each second column of the matrices is multiplied by j , before either the real or imaginary part of the matrices is taken according to (7) or (8). If we plug (4), (7) and (8) into (6) and differentiate with respect to $\boldsymbol{w}_k^{(\mathrm{R})}$ and $\boldsymbol{w}_k^{(\mathrm{I})}$, we end up with

$$\boldsymbol{w}'_{k,\mathrm{MMSE}} = \left[\boldsymbol{H}_k \boldsymbol{R}_x \boldsymbol{H}_k^{\mathrm{T}} + \boldsymbol{F}_k \hat{\boldsymbol{R}}_x \boldsymbol{F}_k^{\mathrm{T}} + \boldsymbol{R}'_{\eta,k}\right]^{-1} \boldsymbol{H}_k \boldsymbol{R}_x \boldsymbol{e}_\nu, \quad (9)$$

with $\boldsymbol{H}_k = \begin{bmatrix} \boldsymbol{G}_k^{(\mathrm{R})} \\ \boldsymbol{G}_k^{(\mathrm{I})} \end{bmatrix}$ and $\boldsymbol{F}_k = \begin{bmatrix} \boldsymbol{M}_k^{(\mathrm{R})} & \boldsymbol{N}_k^{(\mathrm{R})} \\ \boldsymbol{M}_k^{(\mathrm{I})} & \boldsymbol{N}_k^{(\mathrm{I})} \end{bmatrix}$. The correlation matrix of the stationary OQAM modulated input symbols $\boldsymbol{R}_x = \mathrm{E}\left[\boldsymbol{x}_k[n] \boldsymbol{x}_k[n]^{\mathrm{T}}\right] = 0.5\sigma_d^2 \boldsymbol{I}_{L+1}$ — with the variance σ_d^2 of the stationary input symbols $d_k[m]$ — in (9) is identical for all used subcarriers, since we assume that the uncorrelated input symbols have the same statistics and no weighting of subcarriers is performed except for guard carriers with zero input, where $\boldsymbol{R}_x = \boldsymbol{0}_{L+1}$. $\hat{\boldsymbol{R}}_x$ and $\boldsymbol{R}'_{\eta,k}$ represent the correlation matrices

$$\hat{\boldsymbol{R}}_x = \begin{bmatrix} \boldsymbol{R}_x & \boldsymbol{0}_{L+1} \\ \boldsymbol{0}_{L+1} & \boldsymbol{R}_x \end{bmatrix}, \boldsymbol{R}'_{\eta,k} = \begin{bmatrix} \boldsymbol{R}'_{\eta,k,1} & \boldsymbol{R}'_{\eta,k,2} \\ -\boldsymbol{R}'_{\eta,k,2} & \boldsymbol{R}'_{\eta,k,1} \end{bmatrix}, \quad (10)$$

with

$$\boldsymbol{R}'_{\eta,k,1} = 0.5\left(\boldsymbol{\Gamma}_k^{(\mathrm{R})} \boldsymbol{R}_\eta \boldsymbol{\Gamma}_k^{(\mathrm{R}),\mathrm{T}} + \boldsymbol{\Gamma}_k^{(\mathrm{I})} \boldsymbol{R}_\eta \boldsymbol{\Gamma}_k^{(\mathrm{I}),\mathrm{T}}\right) \quad (11)$$

and

$$\boldsymbol{R}'_{\eta,k,2} = 0.5\left(\boldsymbol{\Gamma}_k^{(\mathrm{R})} \boldsymbol{R}_\eta \boldsymbol{\Gamma}_k^{(\mathrm{I}),\mathrm{T}} - \boldsymbol{\Gamma}_k^{(\mathrm{I})} \boldsymbol{R}_\eta \boldsymbol{\Gamma}_k^{(\mathrm{R}),\mathrm{T}}\right). \quad (12)$$

$\boldsymbol{R}'_{\eta,k,2}$ is equal to zero for uncorrelated stationary noise with $\boldsymbol{R}_\eta = \mathrm{E}\left[\boldsymbol{\eta}[l] \boldsymbol{\eta}^{\mathrm{T}}[l]\right] = \sigma_\eta^2 \boldsymbol{I}$ and RRC subcarrier filters $h_k[l]$ at the receiver. The relation between $\boldsymbol{w}'_k$ in (9) and $\boldsymbol{w}_k$ in (6) is given by

$$\boldsymbol{w}_k'^{\mathrm{T}} = \left[\boldsymbol{w}_k^{(\mathrm{R}),\mathrm{T}}, \boldsymbol{w}_k^{(\mathrm{I}),\mathrm{T}}\right] \in \mathbb{R}^{2N}. \quad (13)$$

With the steps from above we have found the analytical solution for the N-tap FIR equalizer yielding the MMSE. In [7] we show how to approach to this solution with adaptive OQAM-LMS equalization.

4. SIMULATION RESULTS

We have simulated the performance of the FBMC system with our proposed per-subcarrier equalizer in a typical 3GPP LTE environment in order to compare it with a CP-OFDM system. We confine ourselves to the case of 10 MHz transmission bandwidth splitted up by $M_0 = 1024$ subcarriers with a subcarrier distance of 15 kHz. Only $D_0 = 600$ subcarriers are occupied for data transmission. The remaining subcarriers are utilized as guard carriers or represent the DC carrier. The parameters from above lead to a sampling frequency of $f_s = 15.36$ MHz. The 3GPP LTE feasibility study [8] recommends a long prefix of duration $T_{cp} = 16.67\mu$s, which corresponds to a prefix length of $N_{cp} = 256$, for multi-cell broadcast and very-large-cell scenarios. In this case only 80 % of a subframe are used for data transmission. For a fair comparison in terms of equal throughput we compensate this loss in data rate by a 32-QAM modulation for the CP-OFDM system compared to a 16-QAM modulation for the FBMC system without CP but per-subcarrier equalizer. This leads to a bandwidth efficiency of 3.6 bit/s/Hz for both systems if we assume an occupied bandwidth of exactly 10 MHz and neglect the increased out-of-band emission caused by the sidelobes of the OFDM modulation.

In order to exclude a too optimistic assessment of the FBMC system, we choose an exponential power delay profile for the radio channel between transmitter and receiver which is adapted to the CP of the OFDM system and maximally challenges the FMBC equalizer. The power delay profile is calculated by

$$p[l] = \exp\left(-\frac{l}{f_s \tau'_{RMS}}\right), \quad l = 0, 1, \ldots, 255, \qquad (14)$$

and leads with $\tau'_{RMS} = 4\,\mu$s to an RMS delay spread of $\tau_{RMS} = 3.4\,\mu$s.

The prefix length N_{cp} strongly boosts the number of subcarriers in OFDM systems in order to prevent the transmission of two much redundancy. In contrast the number of subcarriers in the FBMC system can be chosen more flexibly. By increasing the subcarrier bandwidth and the distance between the subcarriers the same data rate can be achieved with a reduced number of subcarriers. If we reduce the number of subcarriers for instance to $M = 256$ this would mean to transmit 50 % redundancy in the OFDM case with the parameters from above. The FBMC system nonetheless adheres to the defined 3GPP spectrum mask whereas OFDM with $M = 1024$ subcarriers already necessitates further techniques like windowing to reduce the out-of-band emission [8]. The FBMC system on the other hand requires a more powerful equalizer due to the increased frequency selectivity of the channel. The results of the simulation for OFDM and FBMC with the number of subcarriers given in Table 2 are depicted in Fig. 6. The one-tap equalizer of CP-OFDM and the

	M	D	QAM	N_{cp} or N	R	μ
OFDM	1024	600	32	256	1	1
FBMC	1024	600	16	3	1	4.1
	512	300	16	9	2	4.7
	256	150	16	15	4	5.3

Table 2. Parameters for Equal Throughput

equalizers of the FBMC systems have been optimized with respect to MMSE. The curve for CP-OFDM with 16-QAM modulation is provided to offer a reference for perfect equalization. This system

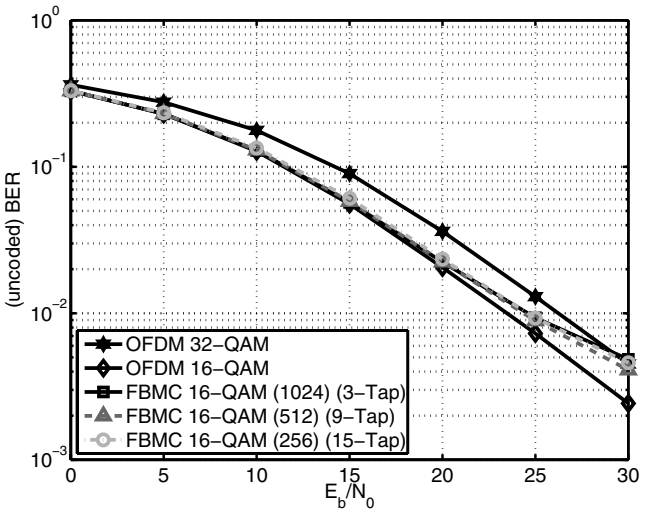

Fig. 6. Comparison of FBMC with CP-OFDM (Modulation Adjusted Such that Both Systems Offer the Same Throughput in Spite of CP

only achieves 80 % of the throughput of all other systems. The results show that the FBMC systems outperform the CP-OFDM 32-QAM system at practical uncoded bit error ratios of 10^{-1} and 10^{-2} by approximately 3 dB and 2 dB with the given equalizer lengths. Note that high E_b/N_0 ratios are necessary due to the sophisticated modulation schemes. The reduction of the subcarriers by the factor R leads to increased subcarrier bandwidths and, consequently, increased frequency selectivity. The results show that a reduction by 2 can be approximately compensated with an extension of the equalizer length by 6 taps. Besides the benefits of FBMC systems compared to OFDM modulation — the smaller out-of-band emission, the suppression of narrowband interferers, easier multiple user access — the reduction of subcarriers and increase of subcarrier bandwidths leads to further noticeable advantages. The sensitivity against carrier frequency offsets is considerably reduced, the time-variation of the propagation channel is less harmful and the problem of high peak-to-average power ratio is alleviated. The total computational complexity is kept fairly constant (cf. Section 4.1 and Table 2). Furthermore, the quality of the equalization can be adjusted by the equalizer length or the equalizer complexity can be adjusted to the channel conditions, respectively. Nonlinear equalization (decision feedback) even improves the results of Fig. 6 in the high E_b/N_0 region because of better interference cancelation. We intend to elaborate on that topic in a further contribution.

The effectiveness of the subcarrier equalization is illustrated in Fig. 7 in the frequency domain. The use of only $M = 256$ subcarriers in the (noise-free) scenario from above leads to a high frequency selectivity, where a one-tap equalizer is obviously overburdened. The upper black contiguous curve is a section of the magnitude response of the radio channel covering 6 of the 150 occupied subcarriers.

Each subcarrier overlaps only with its immediately adjacent subcarriers. The 15-tap per-subcarrier equalizers recover the Nyquist-shaped frequency responses from the distorted subcarriers. This is crucial for the ISI and ICI elimination. It is also interesting to see that the frequency responses are almost flat in the passband region,

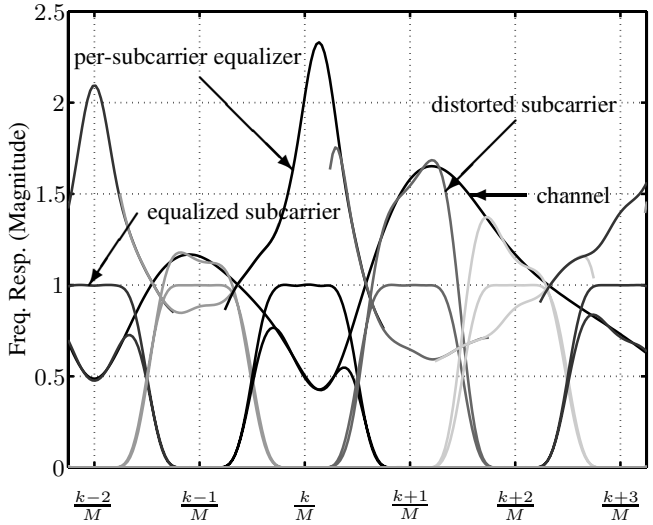

Fig. 7. Illustration of the Equalization of the Subcarriers (FBMC with $M = 256$, noise-free)

which means that the per-subcarrier equalizers also improved the frequency response of the shortly truncated RRC filters with $K = 4$ and a roll-off of $\rho = 0.5$.

The frequency responses of the subcarrier equalizers are as well depicted in Fig. 7 within the stopband edges of the corresponding subcarriers. They complement each other to a curve which is approximately the inverse function of the channel magnitude response.

4.1. Comparison of Complexity

In the following we will define the term "flops" as number of real multiplications per OFDM symbol duration $T = M_0/f_\mathrm{s}$. In order to get a notion of the difference in computational complexity of the OFDM and FBMC system we calculate the number flops for both systems.

If we neglect further complexity to shape the OFDM power spectrum in compliance with spectrum masks OFDM needs $2N_{\mathrm{FFT}}(M)$ flops for the calculation of the IFFT and FFT at transmitter and receiver. There are additionally $4D$ flops for the one-tap equalization at the receiver.

The FBMC system requires altogether $4RN_{\mathrm{FFT}}(M)$ flops for the IFFT and FFT operation at transmitter and receiver, if we use the regular MDFT structure of [9], because the IFFT/FFT operations are executed in $T/2$. Moreover, R "FBMC-symbols" are processed in one OFDM symbol duration T. It is worth mentioning, that this structure could in turn be optimized [4]. The polyphase filters contribute with further $8R(KM+1)$ flops. The equalization takes place with $4RND$ flops.

Equation (15) combines these figures and yields the computational overhead μ of the FBMC system

$$\mu = \frac{N_{\mathrm{FBMC}}}{N_{\mathrm{OFDM}}} = R\frac{N_{\mathrm{FFT}}(M) + 2(MK+1) + ND}{(1/2)N_{\mathrm{FFT}}(M_0) + D_0}. \qquad (15)$$

If we use the split-radix algorithm which computes the M-point FFT/IFFT with $N_{\mathrm{FFT}}(M) = M(\log_2(M) - 3) + 4$ flops and the parameters of the simulation of Section 4 we get the values given in the last column of Table 2.

5. CONCLUSION

In this contribution we have introduced a linear MMSE solution for the equalization of OQAM multicarrier systems. The equalization can also be adapted for single carrier OQAM systems by using the equations for one subcarrier and abandoning the adjacent subcarriers. We have shown that FBMC profits from its high bandwidth efficiency so that it outperforms OFDM systems with CP when compensating for the CP with a higher modulation alphabet. The complexity overhead of FBMC against OFDM occurs in the subcarrier filters and the additional equalizer. We have referred to very efficient implementations of the SFB and AFB. The necessary equalizer length in the simulation setup of this work was not prohibitively high. We show in an other contribution [7] that channel estimation and adaptation of the equalizer to a time-variant channel can also be derived from the solution of this work.

The FBMC system has arbitrary low out-of-band radiation, is more robust against narrowband interference and allows simple multiple user access schemes. At the expense of longer equalizers and slightly increased computational complexity the number of subcarriers can be reduced at least by the factor of 4. This approach increases the robustness against carrier frequency offsets and time-variant channels and alleviates the PAPR problem.

Finally, we would like to point out that the increase of the transmit power in the OFDM case is more expensive than the additional complexity integrated circuits, whose annual technological progress is huge, cope with.

6. REFERENCES

[1] T. Ihalainen *et. al.*, "Channel equalization in filter bank based multicarrier modulation for wireless communications," *EURASIP Journal on Advances in Signal Process.*, 2007.

[2] P. Siohan, C. Siclet, and N. Lacaille, "Analysis and design of OFDM/OQAM systems based on filterbank theory," *IEEE Trans. Signal Process.*, vol. 50, no. 5, pp. 1170–1183, May 2002.

[3] L. G. Baltar, D. S. Waldhauser, and J.A. Nossek, "Out-of-band radiation in multicarrier systems: a comparison," in *Proc. MC-SS Workshop*. May 2007, pp. 107–116, Springer.

[4] T. Karp and N. J. Fliege, "Computationally efficient realization of MDFT filter banks," in *Proc. 8th European Signal Process. Conf.*, September 1996, vol. 2, pp. 1183–1186.

[5] D. S. Waldhauser and J. A. Nossek, "MMSE equalization for bandwidth-efficient multicarrier systems," in *Proc. IEEE Int. Symp. Circuits Syst.*, 21-24 May 2006, pp. 5391–5394.

[6] J. C. Tu, "Optimum MMSE equalization for staggered modulation," in *Conf. Record of The Twenty-Seventh Asilomar Conf. on Signals, Systems and Computers*, Pacific Grove, CA, Nov. 1–3, 1993, pp. 1401–1406.

[7] D. S. Waldhauser, L. G. Baltar, and J. A. Nossek, "Adaptive Equalization for Filter Bank Based Multicarrier Systems," in *Proc. IEEE Int. Symp. Circuits Syst.*, 18-21 May 2008.

[8] Technical Specification Group Radio Access Network, "Feasibility Study for Orthogonal Frequency Division Multiplexing (OFDM) for UTRAN enhancement (release 6)," *3GPP TR 25.892 V6.0.0*, (2004-06).

[9] T. Karp and N. J. Fliege, "Modified DFT filter banks with perfect reconstruction," *IEEE Trans. Circuits Syst. II*, vol. 46, no. 11, pp. 1404–1414, Nov. 1999.